minerals

MDPI

Article

Investigation on the Mineral Catalytic Graphitization of Anthracite during Series High Temperature Treatment

Haiyue Cao, Kuo Li *, Hao Zhang and Qinfu Liu

School of Geosciences and Surveying Engineering, China University of Mining and Technology (Beijing), Beijing 100083, China; chy@student.cumtb.edu.cn (H.C.); zhh199175@outlook.com (H.Z.)
* Correspondence: likuo0818@gmail.com or kuo.li@cumtb.edu.cn

Abstract: Graphite can be artificially converted from anthracites under high temperatures; however, the exact mechanism through which inorganic minerals contribute to the graphitization process is still unknown. In light of this, several selected minerals in different amounts were added to demineralized anthracite coal. The anthracite–mineral mixtures were subjected to artificial graphitization experiments under temperatures ranging from 1700 to 2900 °C in the laboratory. The obtained series of coal-based graphites with various levels of graphitization were characterized by X-ray diffraction (XRD), and the derived structural parameters, such as d_{002} and FWHM (002), La, and Lc were used to compare the carbon structural evolution during the high temperature treatment and mineral catalytic graphitization. Moreover, the amorphous carbon of anthracite is eventually transformed into the highly ordered crystalline carbon of coal-based graphite. The five added minerals show interesting structural variation during the graphitization process, in which pyrite is decomposed into iron (Fe), illite, quartz, and kaolinite, which can react with disordered carbon in organic matter to form moissanite (SiC), while dolomite seems to react with sulfur to form oldhamite (CaS). At temperatures less than 2300 °C, the minerals could significantly enhance the catalytic effect. There is a clear difference in the catalytic effect of different minerals on graphitization. Kaolinite exhibits the strongest catalytic effect. The minerals dolomite, illite, and quartz only show a certain degree of catalysis. Pyrite, however, only has a limited effect on improving the degree of graphitization at a temperature of 1700 °C. However, once the temperature exceeds 2300 °C, the dominant factor controlling the graphitization of anthracite appears to be the temperature. According to the growth pattern at microcrystalline sizes (La and Lc), the minerals' catalytic effects can be classified into three groups. The first group includes minerals that preferentially promote La growth, such as pyrite, illite, and quartz. The second group includes minerals that preferentially promote Lc growth, such as dolomite. Finally, kaolinite is in a separate group that promotes microcrystal growth in both the lateral and vertical directions simultaneously. The mechanisms of the minerals' catalytic graphitization are discussed in this paper. The promotion role of minerals in the artificial graphitization process may help to optimize the graphitization process and reduce the process cost in the future.

Keywords: coal-based graphite; minerals; catalytic graphitization; high-temperature treatment; XRD

Citation: Cao, H.; Li, K.; Zhang, H.; Liu, Q. Investigation on the Mineral Catalytic Graphitization of Anthracite during Series High Temperature Treatment. *Minerals* **2023**, *13*, 749. https://doi.org/10.3390/min13060749

Academic Editor: Yuri N. Palyanov

Received: 29 March 2023
Revised: 22 May 2023
Accepted: 29 May 2023
Published: 31 May 2023

1. Introduction

Synthetic graphite is a highly valuable material with many applications, such as metal smelting, rechargeable batteries, steel-making carburizers, etc. Recently, coal-based artificial graphite has been attracting extensive attention as an anode material for lithium-ion batteries (LIBs) [1–9]. In the synthetic graphite industry, readily graphitized carbons are selected as the raw materials. Currently, petroleum coke is used as the primary filler material in the manufacturing of synthetic graphite. However, as the demand for synthetic graphite has grown, the price of petroleum coke has risen significantly, and the performance of synthetic graphite made from coke is unpredictable, which greatly impedes the industrialization of petroleum coke in order to make artificial graphite materials [3,6,7,10]. Seeking low-cost

and easily available graphitizable carbon materials as replacement for petroleum coke can benefit the synthetic graphite industry's sustainable development.

As a type of high-ranking coal and a natural resource with abundant reserves, anthracite should be considered as an attractive feedstock to produce carbon materials rather than as a fuel [11]. First, most anthracites contain 92%–98% carbon, virtually all of which is present as aromatic carbon molecules in large polycyclic aromatic sheets, resulting in extraordinary properties such as a highly aromatic nature, a low proportion of aliphatic side-chains, and a high ultra-microporosity pore volume [3,6,7,10,12,13]. Second, anthracites are widely recognized as being more highly graphitizable than any other graphitizing carbon investigated at heating to temperatures above 2000 °C [11,12,14]. Additionally, anthracite's relatively low cost, compared to petroleum coke, endows it with a great economic advantage [10].

The fact is that not all anthracites, even those of similar ranks, exhibit the same level of graphitization when heated under the same circumstances [15]. This is mainly related to the organic characteristics of anthracite, such as its microstructure, elemental composition, coalification degree, etc., [6,7,10,12,13,16–26]. Coal itself is a complex geological substance, and it also contains varying proportions of minerals in addition to the main organic matter of the coal body. Minerals are common components in coal, yielding ash when coal is used as fuel, thus contributing to air pollution. Nevertheless, in recent years, coal-based minerals have gained recognition as a potentially valuable source of critical metals [27–29]. The major non-organic elements in the mineral components of coal, such as Fe, Mg, Mn, Si, Al, and Ti, are used as catalysts for graphitization in the production of various carbon materials [30–35].

Previous studies on the role of mineral matter during the graphitization of anthracites have demonstrated that certain minerals have a positive impact on the graphitization of these high-rank coals under high-temperature treatment [12,18,28,36–40]. For instance, González et al. showed that the degree of crystalline organization attained by heat-treated anthracites increases with the amount of mineral content included. The clay mineral illite and iron-containing minerals such as ankerite and siderite usually show good catalytic effects [18]. Pappano et al. further considered that anthracite is graphitizable only if mineral matter is present, and the authors proposed that carbides aid in the graphitization of anthracite [36]. Moreover, it was discovered by Rodrigues et al. that carbide can not only promote the coalescence of crystallites in the La direction but also serve as a catalyst and/or a template for the formation of graphite-like structures [28]. In addition, Tang et al. investigated the catalytic mechanism of Fe on the graphitization of coal via a computer simulation using the ReaxFF force field. These authors believe that catalytic graphitization is explained by the metal–carbide formation–decomposition mechanism and the dissolution-precipitation mechanism [31]. However, some reports have asserted that the catalytic impact of minerals in coal is negligible and even impedes the graphitization of organic matter. Nyathi et al. indicate that aluminum compounds found in anthracite serve as a physical obstacle instead of as a catalyst in the graphitization process [19]. According to Huan et al., the existence of minerals leads to many irregular pore defects in anthracite-based graphene during the high-temperature synthesis of graphite from coal [17]. So, up to now, there has been no unified understanding of how minerals affect the high-temperature graphitization of coal, especially the catalytic graphitization effects of different materials at several controlled graphitization stages.

In this paper, five kinds of minerals (quartz, kaolinite, illite, dolomite, and pyrite) that are commonly contained in coal-bearing strata were chosen as the target minerals. Demineralized anthracite samples with the addition of different amounts of the above-mentioned minerals were heated under high temperatures ranging from 1700 to 2900 °C. The purposes of this paper were to (1) evaluate the catalytic graphitization effects of different minerals on anthracite at different temperatures and (2) uncover the catalytic graphitization reaction process of anthracite by the selected minerals under high-temperature treatment.

2. Samples and Analytical Methods

2.1. Sampling and Demineralizing

The samples used in this study were obtained from the underground Jinzhushan coal mine (JZS) in the Hanpo'ao mining area, which is located in central Hunan Province, China [41,42]. The samples were demineralized following an experimental protocol reported previously [17,19,36,41–43]. Briefly, coal samples were mixed with a mixture of concentrated hydrofluoric (HF, 40%) and hydrochloric acid (HCl, 6 mol/L) in a 1:2.5 volume ratio, heated to 60 °C in a water bath, and kept at a constant temperature for 4 h, after which the solution was washed with deionized water until it was neutral and dried in an oven for recovery. The demineralized anthracite samples were noted as JZSD.

2.2. High Temperature Treatment

In the present study, remineralization of the JZSD samples was performed by individually adding five types of minerals (kaolinite (K), quartz (Q), illite (I), pyrite (P), and dolomite (D)) to the JZSD samples. Some studies have shown that mineral matter has less of an impact on samples with a less than 2% ash yield, but samples with a high ash yield of 17.25% have a higher degree of graphitization. Based on this, we determined the amount of mineral matter to add. The contents of each mineral added into the demineralized samples were 2%, 10%, and 20% (wt%). The graphitization of each demineralized and remineralized sample was carried out using an ultra-high-temperature graphitization furnace. Crucibles containing about 5 g of each powder sample and covered subsequently with lids were fed into the furnace from the top and passed through the high-temperature region, which was inductively heated in an inert atmosphere (Figure 1a,b). The feedstock input and output were continuous operations. These samples were heated to 1700 °C, 2000 °C, 2300 °C, 2600 °C, and 2900 °C at a rising rate of 10 °C/min and kept for 3 h at the set temperature. Afterward, the furnace was naturally cooled to ambient temperature. The high-temperature-treated samples yielded the coal-based graphite products, which were identified by a code that was JZSD plus the mineral content and an abbreviation ending with a heat treatment temperature [17,19,27,28,33,36,44,45]. For example, the products obtained from the demineralized sample and the remineralized sample mixed with 20% kaolinite after heat treatment at 1700 °C were named JZSD-1700 °C and JZSD-20K-1700 °C, respectively. It should be noted that no multiple independent experiments were carried out in this paper because the graphitization equipment is not readily available. A flowchart for this research is shown in Figure 1b.

2.3. X-ray Diffraction Analysis

XRD was carried out using a Rigaku D/MAX-2500PC fully automatic powder diffractometer equipped with a monochromatic Cu Kα X-ray source and an internal standard of silicon power [46,47]. Ni-filtered Cu radiation (λ = 1.54056Å) produced at 40 kV and 100 mA was used for the analysis. Diffraction measurements were recorded by the continuous sweep method at a scanning rate of 2°/min over the interval from 2.5 to 80° in the 2θ range. The XRD patterns were analyzed for structural parameters using the MDI Jade5.0 software. This experiment was completed at the China University of Mining and Technology Beijing. The mean interlayer spacing (d_{002}), was calculated from the location of the (002) peak by using Bragg's equation. The microcrystalline structural parameters were calculated by using Scherrer's equations: $Lc = 0.9\lambda/\beta_{002}\cos(\varphi_{002})$; $La = 1.84\lambda/\beta_{100}\cos(\varphi_{100})$, where φ_{002} and φ_{100} are the peak positions of the (002) and (100) bands, respectively; β_{002} and β_{100} denote the full width at half maximum (FWHM) of the (002) and (100) peaks, respectively. The degree of graphitization (DOG) and the average number of layers <N> were determined by the following equations: $DOG = (3.440\text{-}d_{002})/(3.440\text{–}3.354)$, $\langle N\rangle = Lc/d_{002}$ [17,28,34,41,42,48–51].

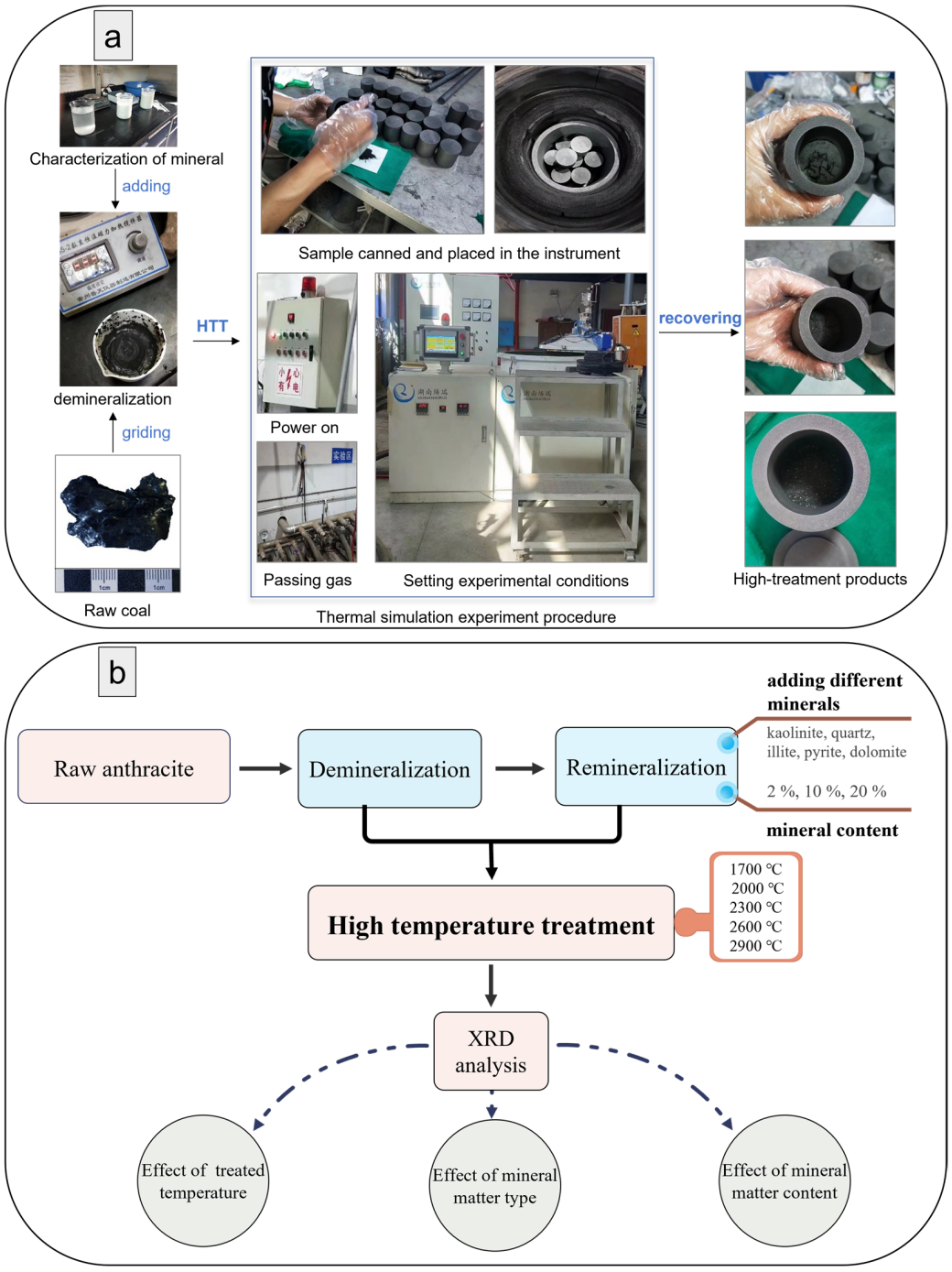

Figure 1. (**a**) Experimental procedures and experimental apparatus for thermal treatment; (**b**) a flowchart of the study.

3. Results

3.1. Characterization of Raw Samples

The samples were crushed to <20-mesh for the petrographic analysis and crushed to <60-mesh for the geochemical analysis [41]. The volatile matter yield of the raw sample was 5.27%, the hydrogen content was 2.19%, and the mean random vitrinite reflectance value was 4.50% (Table 1), indicating the JZS sample was a typical anthracite. According to the textural and morphological features observed under the microscope, the maceral composition of the JZS sample was determined to be 54.5% vitrinite and 45.2% inertinite (Figure 2a,b, Table 1).

Table 1. Geochemical and petrographic characters of the raw JZS anthracite.

Sample	Proximate Analysis (%)				Ultimate Analysis (%)					Macerals (Vol%)		Rr/%
	M_{ad}	A_{ad}	VM_{daf}	FC_{daf}	C_{daf}	H_{daf}	N_{daf}	S_{daf}	O_{daf}	V	I	
JZS	2.15	5.00	5.27	94.73	94.57	2.19	1.08	0.42	1.73	54.5	45.2	4.50

Note: FC, fixed carbon (dry, ash-free basis, daf); VM, volatile matter; M, moisture (air-dried basis, ad); A, ash yield (dry basis, d); V, vitrinite; I, inertinite; Rr, random vitrinite reflectance (% in oil). Data were partially obtained from Li et al. [41].

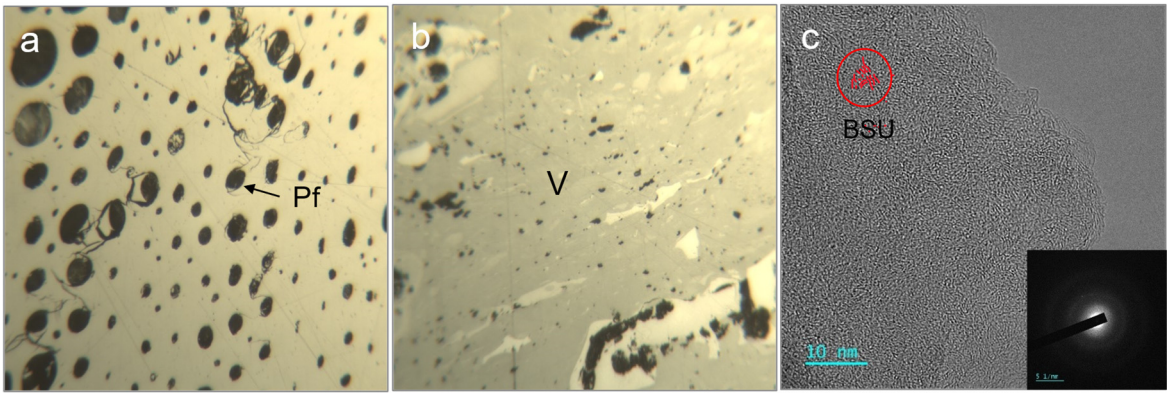

Figure 2. Optical micrograph images and high-resolution transmission electron microscopy images of the JZS sample. (**a**) Pyrofusinite (Pf); (**b**) vitrinite (V); (**c**) basic structural unit (BSU).

HRTEM can reveal the nano-scale carbon structure of coal [19,42,52–54]. In Figure 2c, the HRTEM images of the JZS sample are shown, and the corresponding selected-area electron diffraction (SAED) is inserted. It is possible to discern that the carbon layers that formed the basic structural unit (BSU) were relatively few in number, short in length, rather contorted, and randomly oriented. The electron diffraction patterns showed only one or two diffuse rings, which is typical of the amorphous carbon structure of anthracite.

Information on the structural changes in the raw and demineralized samples were characterized by XRD. The ash yield of the JZS raw anthracite was 5.00%, and the inorganic composition of the raw sample consisted mainly of kaolinite, illite, and ankerite (Figure 3a, low-temperature ashing anthracite sample). The X-ray diffractograms of the samples were typical for anthracite, as shown in Figure 3b, and they exhibited broad 20~30° (002) and 40~45° (100) peaks. It was noticed that many of the sharp mineral peaks in the raw coal disappeared after the acid treatment, suggesting that the demineralization process succeeded.

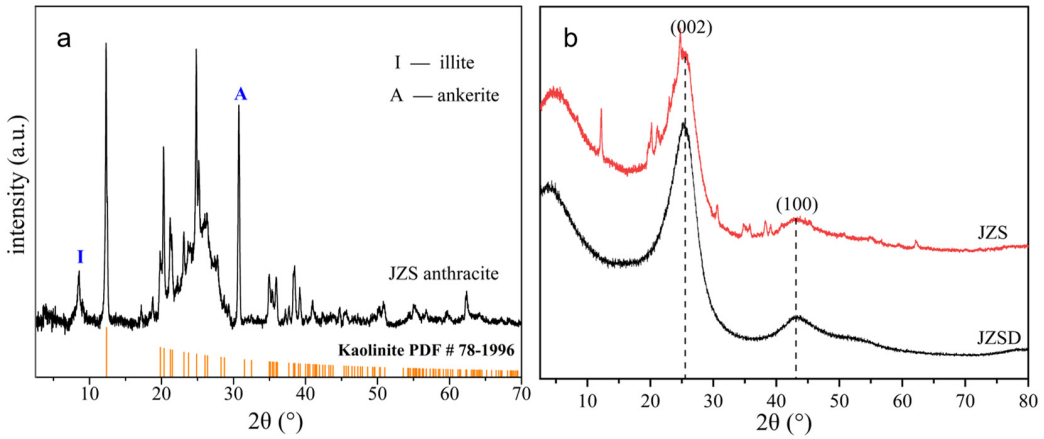

Figure 3. (**a**) Inorganic mineral types in JZS sample; (**b**) XRD comparison graph of raw and demineralized coal samples.

3.2. Effect of Thermal Treatment Temperature

The X-ray diffraction patterns of the pristine demineralized anthracite and the materials obtained from the demineralized anthracite treated at temperatures ranging from 1700 to 2900 °C are depicted in Figure 4. All the samples showed a prominent diffraction peak located at approximately 25~26°, and this band exhibited varied characteristics, from broad asymmetry through sharp asymmetry to sharp symmetry, with increasing the temperature (Figure 4a). Four distinct peaks representing the (002), (100), (004), and (110) diffraction planes were easily detected in the XRD spectra. It is generally accepted that a gradually strengthening (002) diffraction peak intensity and a narrowing peak width indicate that the degree of graphitization and crystallinity increases with increasing the treatement temperature. For the demineralized JZSD sample, its (002) band was deconvoluted into two Gaussian peaks (γ1 and γ2 peaks) located at 18.3° and 25.0°, respectively (Figure 4b). Similarly, the (002) diffraction peak for the JZSD-2000 °C sample was split into two peaks, namely the γ2 and (002) peaks, at approximately 25.2° and 25.8°, respectively, as shown in Figure 4c. The broad γ1 peak at 2θ of the 18–21° band was attributed to amorphous carbon, which only contributed to the background intensity. Some researchers believe that a γ2 peak with a 2θ of 24~25° can be ascribed to graphite-like structures (crystalline carbon), reasoning that the γ2 band represents nano-scaled graphite crystallites, which are attached by other functional groups in the coal structure [55,56]. The peak at ~26° was due to the (002) band of the graphite reflection [50,57–60]. This finding demonstrated that when the temperature rose, the amount of disordered carbon (γ1) and graphite-like carbon (γ2) progressively declined, and the amount of graphite carbon gradually rose. Moreover, starting from a temperature of 2600 °C, the modulated (10) diffraction band in the samples separated into two well-defined (100) and (101) peaks (enlarged image inserted in Figure 4a), which were comparable to the results of natural microcrystalline graphite, as reported previously [41,42,52–54,61,62]. Additionally, two diffraction peaks at 54.5° and 77.43° attributed to (004) and (110), respectively, became clearly visible.

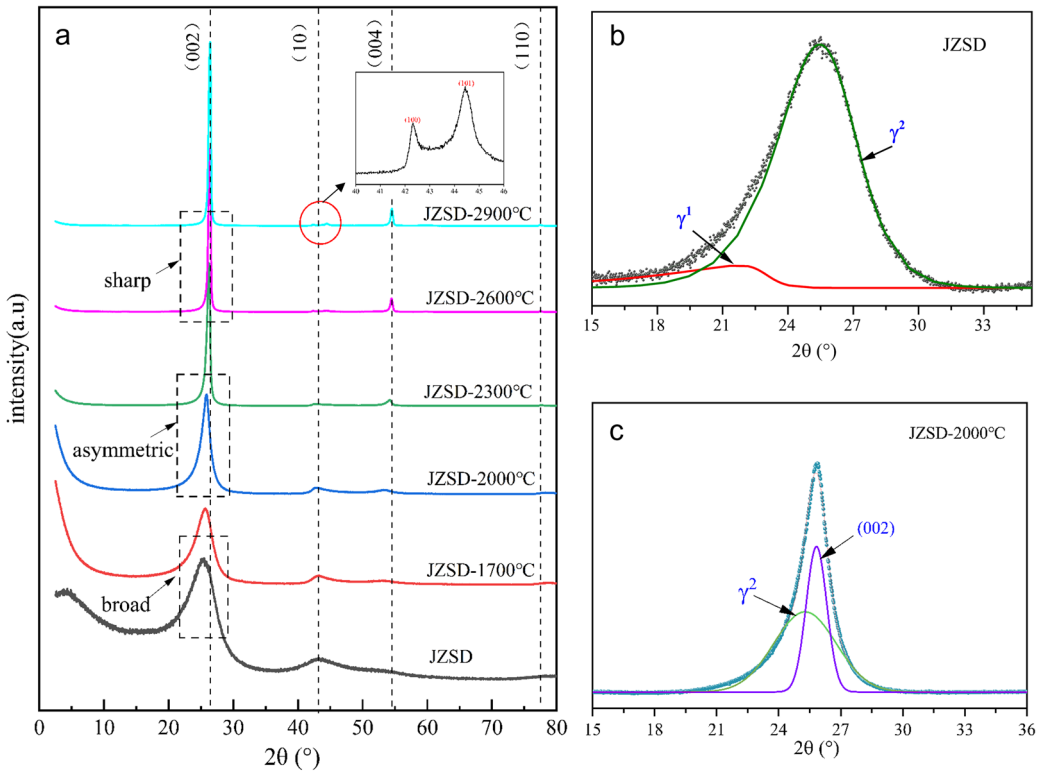

Figure 4. (**a**) XRD patterns of JZSD after different temperature treatments; curve-fitting of (002) peak of (**b**) JZSD and (**c**) JZSD-2000 °C, showing deconvoluted peaks representing γ1, γ2, and (002).

XRD parameters for the series samples were shown in Table 2. The d_{002} spacing gradually decreases from 0.3498 to 0.3380 nm, and the FWHM (002) of the samples progressively reduces from 4.365 to 0.417 (°2θ). In comparison to d_{002}, the variation in FWHM (002) is more regular as the temperature changes, with correlation coefficient R^2 as high as 0.91, while the R^2 after linear fitting of d_{002} is 0.88 (Figure 5a). Therefore, the FWHM (002) seems to more accurately reflect the graphitization degree, similar results also reported by Li et al. for naturally graphitized coals [41]. Furthermore, we also have noticed that the evolution process of microcrystalline sizes La and Lc over temperature accelerates at temperatures above 2000 °C, both with an overall S-shaped growth (Figure 5b). The above XRD data show that temperature is the most important factor for graphitization, as with similar results obtained by previous reports [6,12,14,16,19,23].

Table 2. Structural parameters for demineralized samples at different temperatures and samples with different mineral additions after treatment at 2900 °C.

Samples	d_{002}/nm	FWHM(002)/°2θ	Lc/nm	La/nm	<N>	DOG
JZSD	0.3498	4.365	1.85	5.41	5	—
JZSD-1700 °C	0.3446	2.895	2.79	8.06	8	—
JZSD-2000 °C	0.3452	1.748	4.62	11.89	13	—
JZSD-2300 °C	0.3402	0.620	13.04	25.61	38	0.437
JZSD-2600 °C	0.3385	0.439	18.43	55.95	54	0.643
JZSD-2900 °C	0.3380	0.417	19.4	65.13	57	0.702
JZSD-20K-2900 °C	0.3390	0.433	18.68	55.41	55	0.585
JZSD-20I-2900 °C	0.3382	0.345	23.45	67.92	69	0.673
JZSD-20P-2900 °C	0.3382	0.353	22.92	68.45	68	0.673
JZSD-20Q-2900 °C	0.3387	0.386	20.95	52.89	62	0.614
JZSD-20D-2900 °C	0.3385	0.407	19.87	58.77	59	0.643
JZSD-2K-1700 °C	0.3481	2.748	2.94	10.63	8	—
JZSD-10K-1700 °C	0.3431	2.400	3.37	9.08	10	0.108
JZSD-20K-1700 °C	0.3405	1.067	7.58	29.54	22	0.407
JZSD-2P-2000 °C	0.3449	1.644	4.92	11.16	14	—
JZSD-10P-2000 °C	0.3441	1.608	5.03	13.77	15	—
JZSD-20P-2000 °C	0.3382	0.693	11.67	33.27	35	0.673
ATOD1-2400 °C	0.3448	—	5.0	12.5	—	—
ATO-2400 °C	0.3430	—	6.4	19.5	—	—
ATOD4-2400 °C	0.3398	—	11.0	39.3	—	—

Note: FWHM, full width at half maximum of (002) diffraction peak; Lc and La, crystallite size; <N>, the average number of layers; DOG, degree of graphitization. The last three sample data are cited from previous studies [18].

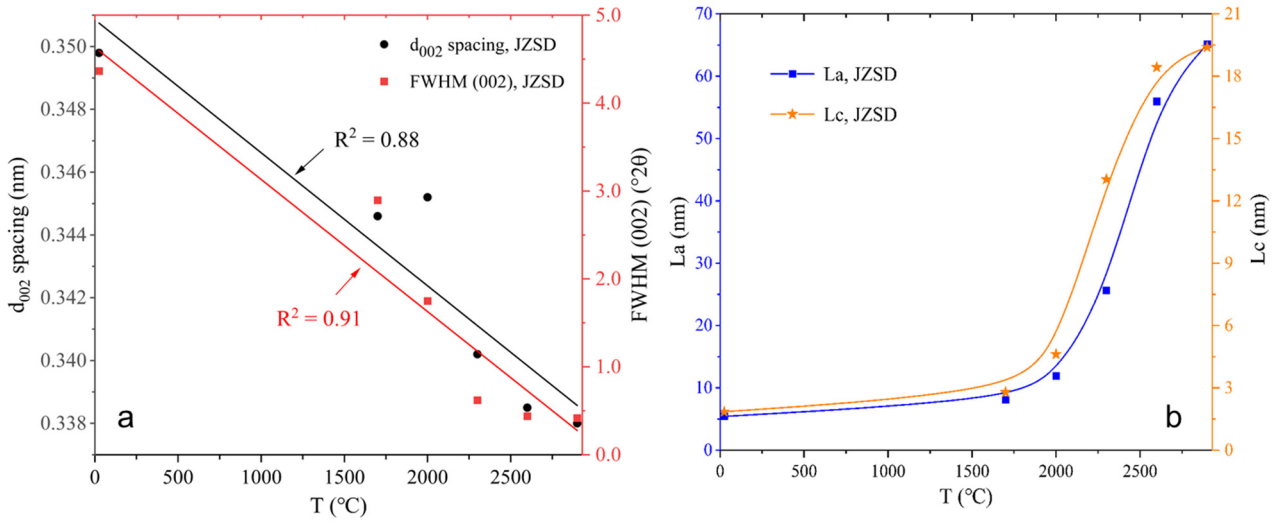

Figure 5. (**a**) The variations in FWHM (002) and d_{002} with increasing temperature; (**b**) the changes in the microcrystalline parameter (La and Lc) with increasing temperature.

3.3. Effect of Mineral Matter Type

The XRD analysis of the series of heated samples was carried out to investigate the effect of the different minerals on the graphitization of anthracite. Kaolinite, illite, and quartz had a high purity, and the other two minerals (pyrite and dolomite) contained small amounts of impurities (Figure 6a). The XRD profiles of the thermal simulation products with the addition of different minerals after the heat treatment at 1700 °C are shown in Figure 6b. Although the (002) diffraction peaks of each sample were clear and obvious, the peak shapes showed different characteristics, among which the JZSD sample with added kaolinite showed the sharpest and strongest (002) band and also showed (101) and (110) peaks, indicating a three-dimensional structural order. The samples with dolomite and illite had a relatively broader (002) peak than the JZSD-20K-1700 °C sample, whereas the samples containing quartz and pyrite showed broad, weak (002) diffraction peak intensities, as shown at the bottom of Figure 6b. The above phenomena indicated that the addition of the different minerals affected the orderly arrangement of the organic matter during the graphitization process, in which the minerals (especially kaolinite) showed a prominent promotion of graphitization. In addition, the non-graphite phases (moissanite (SiC), oldhamite (CaS), and iron) were identified by XRD in the samples treated at 1700 °C, as shown in Figure 6b. For the samples treated at 2900 °C, there were no significant differences in the XRD patterns of the samples with the different added minerals, all of which showed characteristic diffraction peaks of graphite and were almost free of impurities peaks (Figure 6c). Table 2 also shows that all the graphitized samples at 2900 °C had d_{002} values that were only slightly greater than the well-crystallized graphite layer spacing (0.3354 nm). However, the samples with different added minerals showed different crystallite sizes (La and Lc) and average number of stacked layers (<N>) after graphitization at 2900 °C. As a result, the degree of graphitization for anthracite was regulated by the final heating temperature, whereas the mineral type affected the final crystallite size.

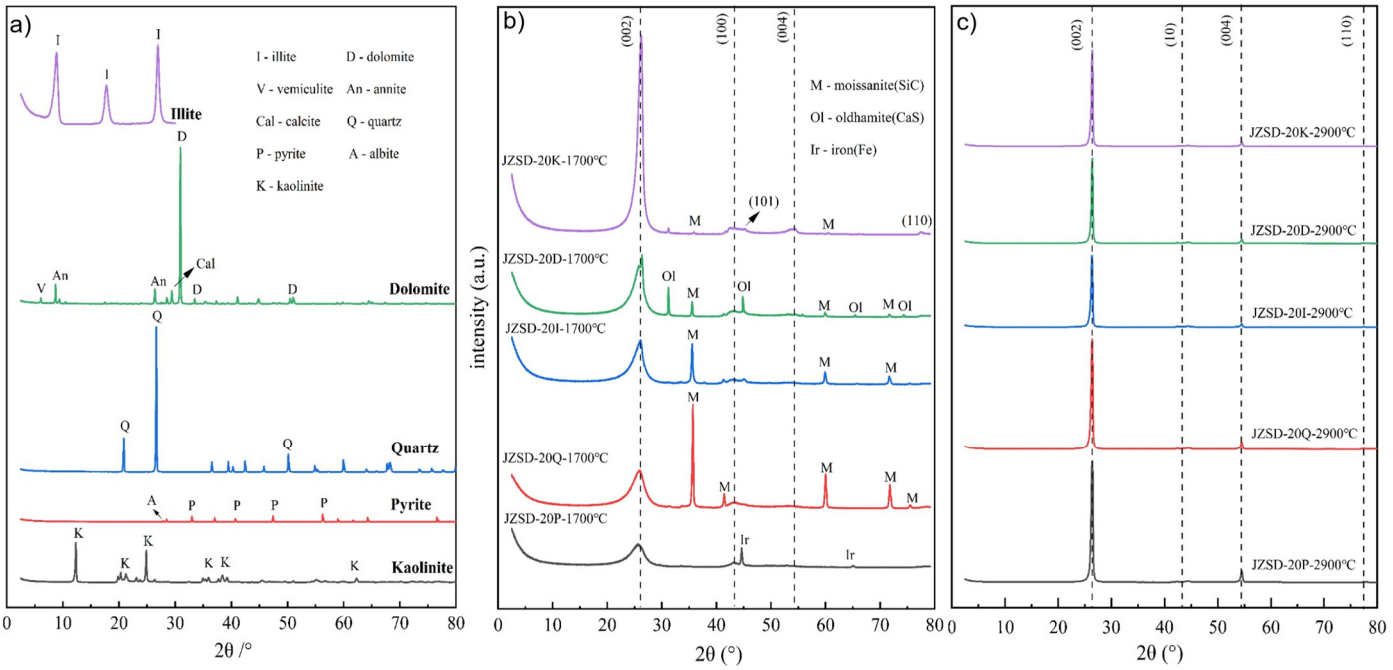

Figure 6. (**a**) XRD spectra of original minerals; JZSD sample with 20% content of different minerals after graphitization at different temperatures: (**b**) 1700 °C; (**c**) 2900 °C.

In Figure 7, the type of mineral matter is plotted against the d_{002} (nm) and FWHM (002) values of the heat-treated materials at 1700 °C. It was found that the layer spacing of all the samples with minerals added, except for pyrite, showed a decreasing trend (Figure 7a), while the FWHM values of all the samples with different minerals added decreased in all

cases, as shown in Figure 7b. The JZSD-20K sample displayed the sharpest (002) diffraction peak, as shown in Figure 6b, along with noticeable (101) and (110) peaks. The JZSD-20P-1700 °C sample had the largest d_{002} (0.3475nm) value despite having a lower FWHM (002) value than the demineralized coal sample JZSD-1700 °C, indicating that the presence of pyrite had little impact on the graphitization and even increased the interlayer spacing. Dolomite, illite, and, lastly, quartz all had a certain degree of catalysis for graphitization but were much less effective than kaolinite.

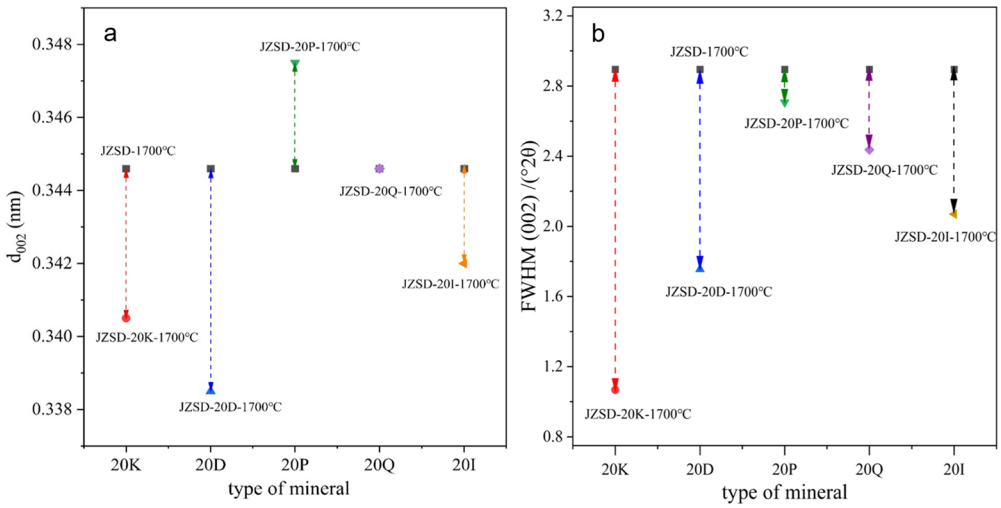

Figure 7. The relationship between the type of mineral matter and XRD parameters for the heat-treated materials at 1700 °C: (**a**) d_{002}; (**b**) FWHM (002). The dashed lines with arrows show the extent of catalytic graphitization level compared to the demineralized sample.

The association between the mineral species and the corresponding crystallite parameters (La and Lc) of the samples treated at 1700 °C is depicted in Figure 8. It should be noted that the La and Lc values of the demineralized samples were the lowest values compared to those of the samples with added minerals. This demonstrated that under the influence of temperature, the minerals underwent phase changes and contributed to the growth of graphite microcrystals, although each mineral did so in a unique manner. It was noted that the microcrystal size increased significantly in the presence of kaolinite (Figure 8), which was also evidenced by our HRTEM images of the JZSD-20K-1700 °C sample shown in the Supplementary Material. This may be related to the interaction between kaolinite and organic matter at certain temperatures, the exact reaction mechanism of which is not currently known. Based on the relationship between the crystalline parameters and mineral type (Figure 8), it was found that dolomite promoted development along the c (stacking) direction over the lateral direction, whereas pyrite showed the opposite effect.

3.4. Effect of Mineral Matter Content

Figure 9a displays the XRD patterns of the heat-treated samples with added quantities of minerals. It was observed that the (002) diffraction peaks gradually became sharp and symmetrical with the increase in the content of kaolinite and pyrite under the same heat treatment conditions. In particular, the XRD features of the JZSD-20K-1700 °C sample had an even higher graphitization degree than those of the samples with 2% and 10% added pyrite treated at 2000 °C (Figure 9a). The measured FWHM (002) value (1.067) of the JZSD-20K-1700 °C sample was lower than that of the JZSD-2P-2000 °C (1.644) and JZSD-20P-2000 °C (1.608) samples. Combined with the performance of the pyrite-added samples at 1700 °C, it was demonstrated that the different minerals had different catalytic action temperature points, and a suitably high percentage of mineral content (20%) effectively accelerated the conversion of organic matter to graphite, which was consistent with the conclusions obtained from a previous study [18]. For example, the degree of

graphitization of the ATOD4 sample (ash = 19.07 wt%) was higher than that of the ATOD1 (ash = 2.07 wt%) and ATO (ash = 10.12 wt%) samples after heat treatment at 2400 °C, as shown in Table 2.

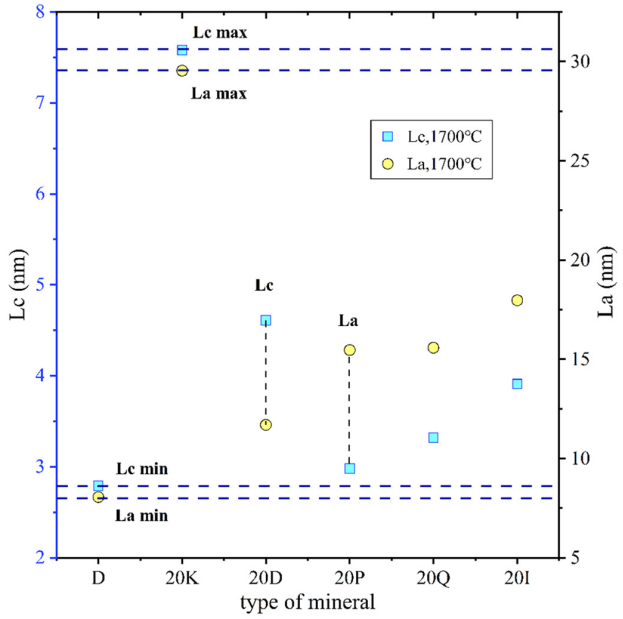

Figure 8. The relationship between the type of mineral matter and crystallite size for the heat-treated materials at 1700 °C.

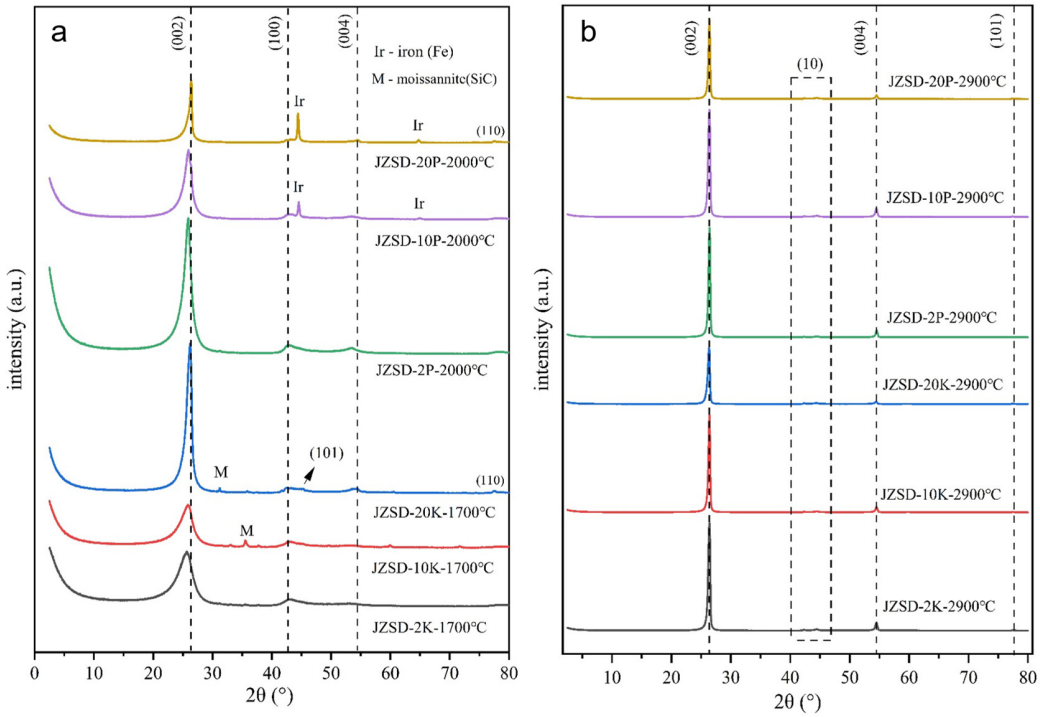

Figure 9. (**a**) XRD diffraction patterns of products after heat treatment with various kaolinite and pyrite contents at 1700 °C and 2000 °C, respectively; (**b**) XRD diffraction patterns of products after heat treatment with various kaolinite and pyrite contents at 2900 °C.

Graphite powder could be obtained under the conditions with a temperature of 2900 °C for all the samples with added kaolinite or pyrite contents of 2%, 10%, and 20%. The XRD patterns used to characterize the graphite powder showed that the only phase was graphite after being treated at 2900 °C (Figure 9b). The new phases formed by mineral

decomposition or reaction with disordered carbon were not visible in the final products or were undetectable due to their extremely low content, indicating that under ultra-high temperature conditions, regardless of the mineral content, they eventually escaped from the reaction system. Based on the aforementioned phenomena, it can be concluded that the mineral content of the raw coal had a significant impact on the final product's microstructure but not on its degree of graphitization. A similar conclusion was also reported by Qiu et al., who found that the crystal structure of the final graphite, either single crystal or polycrystalline, may depend on the content of minerals in the original anthracite [44].

When the mineral content percentages were plotted against the X-ray parameter FWHM (002) in Figure 10, it was observed that the best-ordered materials were obtained from the samples with 20% added kaolinite after heat treatment up to 1700 °C, and the FWHM (002) of all the samples showed a regular variation with increasing the mineral content, except for the samples with pyrite. A linear fit was performed separately for the different minerals, as shown in Figure 10. There appeared to be little or no influence of the content of pyrite on the structural properties of the obtained material (R^2 = 0.02). However, the samples marked with boxes in Figure 10 that had a 2% pyrite addition, in contrast to the samples with the same quantity of other minerals added, had the smallest FWHM (002) value after the heat treatment. This was consistent with other studies that claimed that samples with ash contents below 2% did not exhibit a significant catalytic effect of the mineral matter [12,28]. Additionally, it was noted that the structural order of the obtained materials gradually improved as the content of kaolinite, dolomite, or illite increased. There was a strong correlation between the content of these three types of minerals and the degree of graphitization, with correlation coefficients, R^2, greater than 0.9 (R^2 = 0.98 for illite, R^2 = 0.94 for kaolinite, and R^2 = 0.92 for dolomite) being obtained. Furthermore, the conversion of organic matter to graphite was made easier by the high quartz content, and the formation and decomposition of silicon carbide were intimately tied to the graphitization process [27,28,36]. Therefore, it was concluded that increasing the concentration of the three minerals (kaolinite, dolomite, and illite) under high-temperature conditions < 1700 °C could significantly speed up the graphitization process and lower the initial graphitization temperature.

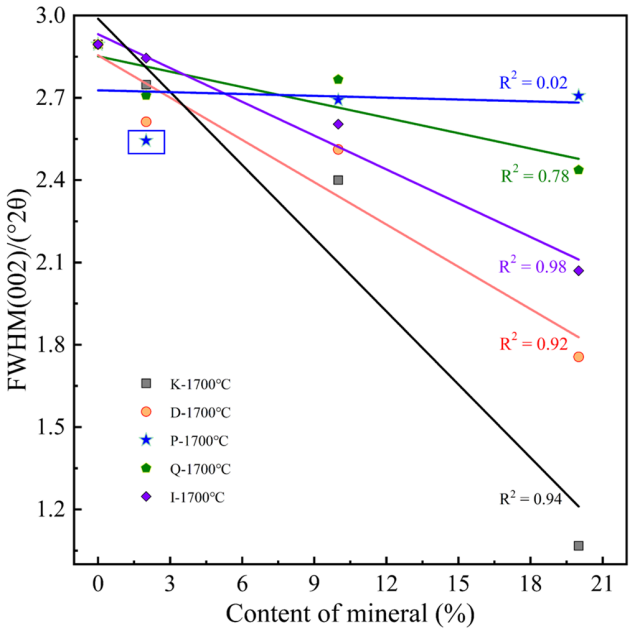

Figure 10. The changes in crystallinity parameter FWHM (002) with increasing the content of mineral matter. Linear fitting line and the coefficient R^2 are shown.

4. Discussion

The differences in the structural and graphitization degree of the samples with different minerals added were probably due to the composition and structural features of the minerals. Therefore, it was necessary to investigate how the minerals affected the growth of the microcrystals during the graphitization process. The La/Lc value can be used to depict the priority growth along the basal plane and vertical direction during graphitization under high-temperature treatment. Larger La/Lc values indicate that the layers tend to extend, and smaller La/Lc values indicate that the layers tend to stack. The variations in the La/Lc values of the demineralized samples and samples with 20% different minerals added under high-temperature treatment are shown in Figure 11a. It was found that when the temperature was 1700 °C, the La/Lc values of the set of samples were more scattered than those at other temperatures, indicating that the minerals had different catalytic graphitization effects at this temperature (Figure 11a). The relationship between the La/Lc value and the mineral species at 1700 °C is depicted in Figure 11b. A high La/Lc value implies that the layers tend to extend along the basal planes, whereas a low La/Lc value suggests that the layers tend to stack vertically [63]. It was observed that the La/Lc values of all the samples were between 2.5 and 5.5, and the La/Lc values made it possible to group the samples into three types (Figure 11b). The first type of samples grew preferentially along the basal plane during the graphitization, with their La/Lc values distributed in the range from 4.5 to 5.2, including the JZSD-20P-1700 °C, JZSD-20Q-1700 °C, and JZSD-20I-1700 °C samples. The second category contained only one sample, JZSD-20K-1700 °C, with an La/Lc value of 3.9. The third group of samples with La/Lc values below 2.89 contained two samples, JZSD-1700 °C and JZSD-20D-1700 °C, and more preferentially formed the microcrystalline column described by Oberlin et al. [13].

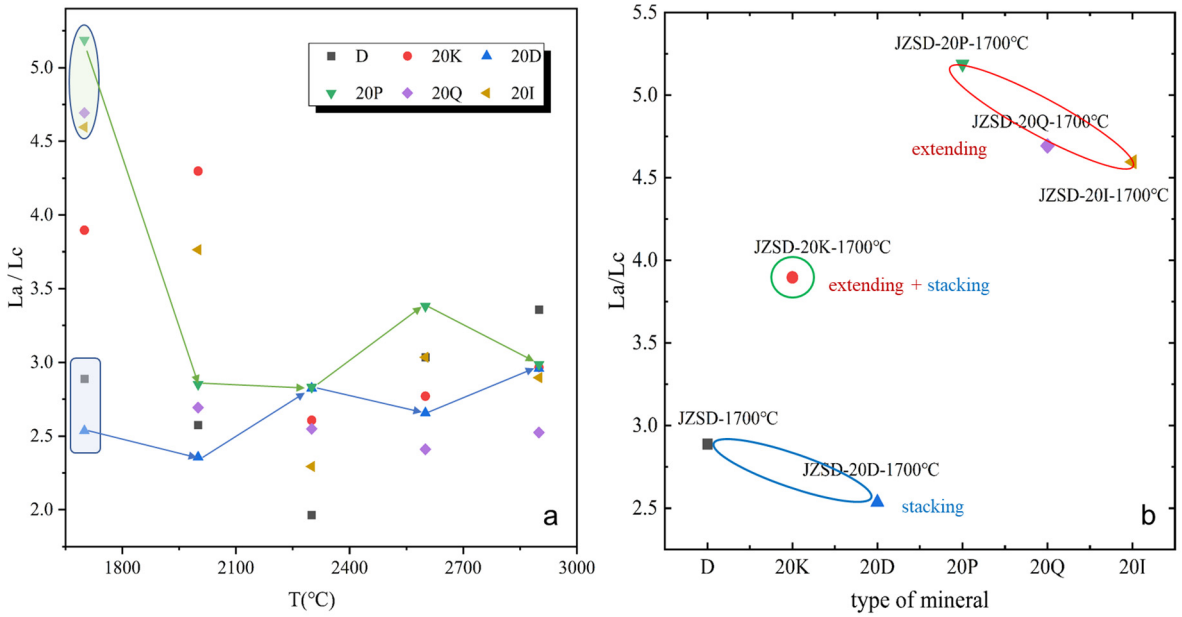

Figure 11. (**a**) The La/Lc values of demineralized and samples with 20% different minerals added changed with the increase in heat treatment temperature. (**b**) The relationship between the type of mineral matter and La/Lc value.

The catalytic effect of minerals is significantly influenced by their physical and chemical properties. For instance, the temperature at which a mineral decomposes plays a crucial role in its catalytic activity. Kaolinite decomposes at 600–650 °C, illite at 850 °C, pyrite at 520–950 °C, dolomite at 750 °C, and quartz is chemically stable with a high melting point of about 1600 °C. In some cases, the complete removal of catalysts during low-temperature graphitization at 1700 °C may not be possible due to certain mineral elements interacting with carbon, leading to the formation of carbides that only break down at high tempera-

tures. In the process of graphite formation, the role of quartz has been studied by some scholars [44,55,56]. The research shows that molten quartz reacts with disordered carbon to form silicon carbide with a structure similar to graphite. This generated SiC can decompose into graphite and silicon under sustained high-temperature conditions. Therefore, the formation and decomposition reactions of silicon carbide are the true mechanism for quartz catalyzing the graphitization of anthracite. In addition, adjusting the quartz content can affect the crystal structure of coal-based graphite products. Research on the catalytic graphitization of anthracite with the addition of illite and kaolinite is relatively scarce and will be detailed in the future. Below, the roles of dolomite and pyrite in the graphitization process of anthracite are discussed in detail.

Dolomite is a binary composite carbonate of $MgCO_3$ and $CaCO_3$. Qian et al. researched the thermal decomposition of dolomite in an Ar atmosphere and found that the products of the thermal reaction are MgO and $Ca(OH)_2$, which are deliquesced by CaO [64]. Subsequently, $Ca(OH)_2$ is decomposed into CaO at a higher temperature.

$$CaMg\ (CO_3)_2 \rightarrow CaO + MgO + 2CO_2 \quad (1)$$

$$CaO + H_2O \rightarrow Ca(OH)_2 \quad (2)$$

$$Ca(OH)_2 \rightarrow CaO + H_2O \quad (3)$$

The literature shows that the presence of calcium oxide during the pyrolysis of coal significantly increases the yield of gas, and magnesium has been used as a catalyst to graphitize anthracite at low temperatures [30,65]. Therefore, it is speculated that the decomposition of dolomite will destroy the C-H bonds of aromatic hydrocarbons and accelerate the dehydrogenation in the graphitization process. Moreover, CaS was identified in the JZSD-20D-1700 °C sample. Guan et al. found that $Ca(OH)_2$ and CaO were quite effective at capturing sulfur in the gaseous phase as CaS [66]. It can be inferred that the organic S in anthracite is precipitated as H_2S and reacts with CaO at temperatures below 1700 °C.

$$CaO + H_2S \rightarrow CaS + H_2O \quad (4)$$

There are active cleavage sites on the inner and outer surfaces of calcium oxide, and its polarity affects the stability of the condensed aromatic ring's electron cloud, which may be the reason why calcium oxide reacts with sulfur-containing functional groups. Moreover, on the nanometer scale, it was observed that graphite nanocrystals with thick stacking layers and three graphite single crystals with different orientations that underwent vertical merging coexisted, as shown on the right side of Figure 12. In addition, the La/Lc value of the JZSD-20D-1700 °C sample was lower than that of the JZSD-1700 °C sample, as shown in Figure 11a. The above phenomena showed that the JZSD-20D-1700 °C sample tended to be stacked vertically, and the vertical stacking continued until 2000 °C (Figure 11a). In addition, CaS was unable to remain stable in the reaction system as the temperature was increased to 2000 °C, indicating that dolomite had a small catalytic effect at ultra-high temperatures.

The samples with pyrite added showed an opposite structural growth priority (Figure 11). Pyrite is the most abundant and dominant sulfide compound in coal. It is generally agreed that the decomposition of pyrite occurs in steps over the temperature range 520–950 °C, but only 70% of pyrite is reduced to Fe at 950 °C [67]. Chen et al. suggest that the hydrocarbons of coal can promote the reduction of pyrite in pyrolysis [67].

$$FeS_2\ (pyrite) \rightarrow FeS_{1.2}\ (pyrrhotite) \rightarrow FeS \quad (5)$$

$$FeS + H_2 \rightarrow Fe + H_2S \quad (6)$$

Srinivasan et al. investigated the effect of pyrite on free radical formation in coal by electron spin resonance spectroscopy and concluded that the formation of free radicals in coal is facilitated by the pyrite-to-pyrrhotite conversion mechanism and by the presence of pyrrhotite itself [68]. In addition, this study found the presence of an iron phase in the JZSD-20P-1700 °C and JZSD-20P-2000 °C samples (Figures 9a and 6b), but it also found a continuous increase in the microcrystalline length La in the series of JZSD-20P samples at temperatures of 1700–2600 °C (Figures 11a and 13). It was therefore presumed that the sulfur in the pyrite spilled out as a gas rather than as sulfur incorporated into organic matter under high temperatures and that the formation of iron continued to promote the graphitization of the organic matter. Some related studies have shown that amorphous carbon has a good solubility in iron, and iron can permeate through organic matter in a liquid phase [31,38,45]. Amorphous carbon near liquid iron is consistently dissolved and arranged in an orderly manner, and it precipitates as graphite at higher temperatures, thus accelerating the graphitization of organic matter. Tang et al. argue that Fe promotes the integration of irregular five- and seven-membered rings into two regular aromatic six-membered rings and that these two processes continue in the process of catalytic graphitization [31]. Based on the above phenomena, the authors suggest that the mechanism of the pyrite-catalyzed graphitization of anthracite is that the decomposition of pyrite at lower temperatures (~950 °C) allows sulfur to escape as H_2S or SO_2, while the removal of heteroatoms from the edges of graphite microcrystals in organic matter, such as the basic structural units (BSUs) or the molecular orientation domains (MOD), leads to the formation of a large number of free radicals. As the temperature increases, the newly generated iron is locally oriented by dissolving amorphous carbon or reacting with carbon to form metal carbides, thus promoting the growth of graphite microcrystals along the La direction in a selective manner and the lateral coalescence of a large number of carbon radicals. Furthermore, this catalysis occurs throughout the graphitization process until ultra-high-temperature conditions (the boiling point of iron is 2750 °C), at which point the iron escapes from the system as a gas phase and the graphite microcrystals undergo vertical stacking (Figures 11a and 13).

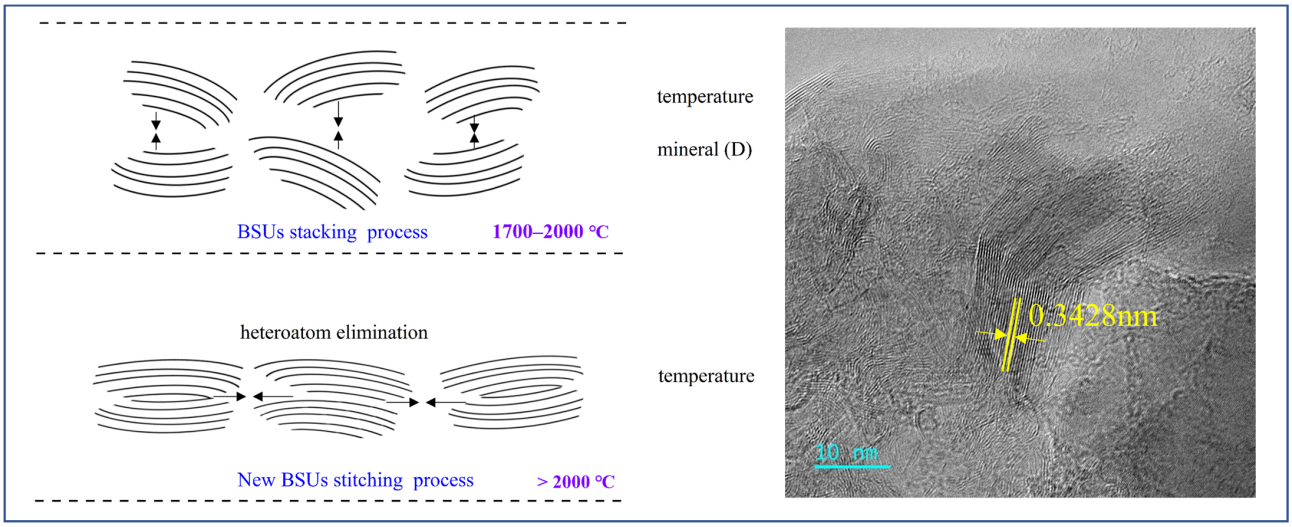

Figure 12. Schematic diagram of the production of synthetic graphite by the action of dolomite. The arrows indicate the direction of movement of the aromatic layer.

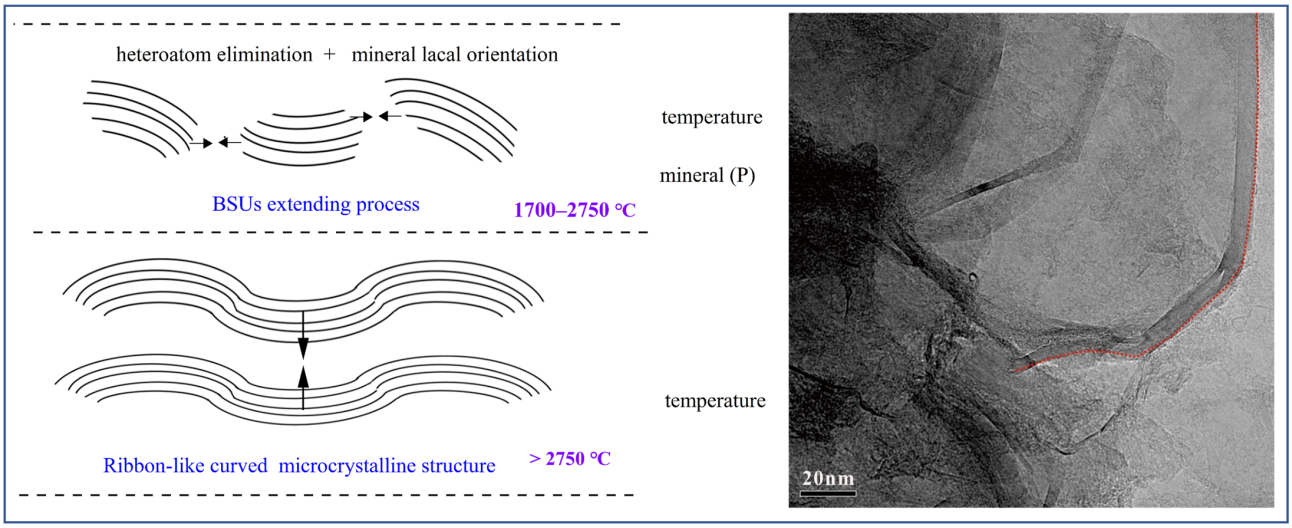

Figure 13. The schematic diagram for the production of synthetic graphite by the action of pyrite. The arrows indicate the direction of movement of the aromatic layer.

5. Conclusions

In this study, a series of coal-based graphite samples synthesized from anthracite with minerals as catalysts were mainly examined using X-ray diffractograms (XRD). The following findings were found based on the series of single high-temperature-run samples:

(1) For the sample series without adding additional minerals (the JZSD series), the crystallite sizes of these samples showed an increasing trend with the treatment temperature. The differences in the structure of the samples treated with different minerals added were observed from the earliest stages of graphitization (1700~2000 °C) and were mainly attributed to the composition and content of the minerals. In addition, an appropriate increase in the mineral content could effectively decrease the initial graphitization temperature of organic matter and accelerate the graphitization process.

(2) The La/Lc parameters made it possible to group the samples after the heat treatment with the addition of different minerals into three main groups: (i) the JZSD-20P-1700 °C, JZSD-20I-1700 °C and JZSD-20Q-1700 °C group; (ii) the JZSD-20D-1700 °C group; and (iii) the JZSD-20K-1700 °C group. In terms of the minerals selected for this experiment, the dolomite favored the vertical stacking of organic aromatic layers, while three minerals, pyrite, quartz, and illite, favored the lateral extension of aromatic layers. The highest degree of graphitization was observed in the kaolinite, and the kaolinite could promote microcrystal growth both in the lateral and vertical directions simultaneously.

(3) The dolomite could accelerate the vertical stacking of graphite microcrystals, probably through dehydrogenation and sulfur fixation at temperatures ranging from 1700~2000 °C, but as the temperature increased, the dolomite had a diminishing effect. The decomposition of the pyrite could aid in forming a large number of free radicals by removing heteroatoms at the edge of the basic structural units or molecular orientation domains, while the newly generated iron probably promoted the preferential growth of graphite microcrystals along the La direction.

Supplementary Materials: The following supporting information can be downloaded at: https://www.mdpi.com/article/10.3390/min13060749/s1, Figure S1: The HRTEM image of the JZSD-20K-1700 °C sample.

Author Contributions: Data curation, H.C.; software, H.C.; investigation, H.C.; validation, H.Z. and H.C.; formal analysis, H.C.; writing—original draft preparation, H.C.; writing—review and editing, H.C. and K.L.; supervision, Q.L. All authors have read and agreed to the published version of the manuscript.

Funding: This research was supported by the National Natural Science Foundation of China (Grant No.42002187) and the Fundamental Research Funds for the Central Universities (2022XJDC01).

Data Availability Statement: Not available.

Acknowledgments: The authors acknowledge support for the samples from the Jinzhushan mine. Sincere thanks are given to Hunan Xirui Automation Equipment Co. Ltd. for providing the high-temperature experimental equipment.

Conflicts of Interest: The authors declare no conflict of interest.

References

1. Li, Y.; Tian, X.D.; Song, Y.; Yang, T.; Wu, S.J.; Liu, Z.J. Preparation and lithium storage of anthracite-based graphite anode materials. *New Carbon Mater.* **2022**, *37*, 1163–1169. [CrossRef]
2. Deng, R.Y.; Chu, F.L.; Yu, H.Y.; Kwofie, F.; Qian, M.Z.; Zhou, Y.; Wu, F.X. Electrochemical performance of expanded graphite prepared from anthracite via a microwave method. *Fuel Process. Technol.* **2022**, *227*, 107100. [CrossRef]
3. Shi, M.; Song, C.L.; Tai, Z.G.; Zou, K.Y.; Duan, Y.; Dai, X.; Sun, J.J.; Chen, Y.Z.; Liu, Y.N. Coal-derived synthetic graphite with high specific capacity and excellent cyclic stability as anode material for lithium-ion batteries. *Fuel* **2021**, *292*, 120250. [CrossRef]
4. Wang, T.; Wang, Y.B.; Cheng, G.; Ma, C.; Liu, X.J.; Wang, J.T.; Qiao, W.M.; Ling, L.C. Catalytic Graphitization of Anthracite as an Anode for Lithium-Ion Batteries. *Energy Fuels* **2020**, *34*, 8911–8918. [CrossRef]
5. Camean, I.; Lavela, P.; Tirado, J.L.; Garcia, A.B. On the electrochemical performance of anthracite-based graphite materials as anodes in lithium-ion batteries. *Fuel* **2010**, *89*, 986–991. [CrossRef]
6. Gonzalez, D.; Montes-Moran, M.A.; Garcia, A.B. Graphite materials prepared from an anthracite: A structural characterization. *Energy Fuels* **2003**, *17*, 1324–1329. [CrossRef]
7. Gonzalez, D.; Montes-Moran, M.A.; Suarez-Ruiz, I.; Garcia, A.B. Structural characterization of graphite materials prepared from anthracites of different characteristics: A comparative analysis. *Energy Fuels* **2004**, *18*, 365–370. [CrossRef]
8. Krebbers, L.T.T.; Lottermoser, B.G.G.; Liu, X. Computed Tomography of Flake Graphite Ore: Data Acquisition and Image Processing. *Minerals* **2023**, *13*, 247. [CrossRef]
9. Xing, B.; Zhang, C.; Cao, Y.; Huang, G.; Liu, Q.; Zhang, C.; Chen, Z.; Yi, G.; Chen, L.; Yu, J. Preparation of synthetic graphite from bituminous coal as anode materials for high performance lithium-ion batteries. *Fuel Process. Technol.* **2018**, *172*, 162–171. [CrossRef]
10. Andresen, J.M.; Burgess, C.E.; Pappano, P.J.; Schobert, H.H. New directions for non-fuel uses of anthracites. *Fuel Process. Technol.* **2004**, *85*, 1373–1392. [CrossRef]
11. Adamczyk, Z.; Komorek, J.; Bialecka, B.; Calus-Moszko, J.; Klupa, A. Possibilities of Graphitization of Unburned Carbon from Coal Fly Ash. *Minerals* **2021**, *11*, 1027. [CrossRef]
12. Oberlin, A.; Terriere, G. Graphitization studies of anthracites by high resolution electron microscopy. *Carbon* **1975**, *13*, 367–376. [CrossRef]
13. Oberlin, A. Carbonization and graphitization. *Carbon* **1984**, *22*, 521–541. [CrossRef]
14. Franklin, R.E. Crystallite growth in graphitizing and non-graphitizing carbons. *Proc. R. Soc. London. Ser. A. Math. Phys. Sci.* **1951**, *209*, 196–218. [CrossRef]
15. Li, R.; Tang, Y.; Che, Q.; Ma, P.; Luo, P.; Lu, X.; Dong, M. Effects of Coal Rank and Macerals on the Structure Characteristics of Coal-Based Graphene Materials from Anthracite in Qinshui Coalfield. *Minerals* **2022**, *12*, 588. [CrossRef]
16. Atria, J.V.; Rusinko, F.; Schobert, H.H. Structural ordering of Pennsylvania anthracites on heat treatment to 2000–2900 degrees C. *Energy Fuels* **2002**, *16*, 1343–1347. [CrossRef]
17. Huan, X.; Tang, Y.G.; Xu, J.J.; Lan, C.Y.; Wang, S.Q. Structural characterization of graphenic material prepared from anthracites of different characteristics: A comparative analysis. *Fuel Process. Technol.* **2019**, *183*, 8–18. [CrossRef]
18. Gonzalez, D.; Montes-Moran, M.A.; Garcia, A.B. Influence of inherent coal mineral matter on the structural characteristics of graphite materials prepared from anthracites. *Energy Fuels* **2005**, *19*, 263–269. [CrossRef]
19. Nyathi, M.S.; Clifford, C.B.; Schobert, H.H. Characterization of graphitic materials prepared from different rank Pennsylvania anthracites. *Fuel* **2013**, *114*, 244–250. [CrossRef]
20. Wang, L.; Qin, R.; Li, Y.; Zhang, H. On the difference of graphitization behavior between vitrinite- and inertinite-rich anthracites during heat treatment. *Energy Sources Part A-Recovery Util. Environ. Eff.* **2022**, *44*, 4991–5003. [CrossRef]
21. Rodrigues, S.; Suarez-Ruiz, I.; Marques, M.; Flores, D.; Camean, I.; Garcia, A.B. Development of graphite-like particles from the high temperature treatment of carbonized anthracites. *Int. J. Coal Geol.* **2011**, *85*, 219–226. [CrossRef]
22. Rodrigues, S.; Suarez-Ruiz, I.; Marques, M.; Camean, I.; Flores, D. Microstructural evolution of high temperature treated anthracites of different rank. *Int. J. Coal Geol.* **2011**, *87*, 204–211. [CrossRef]
23. Zeng, H.; Xing, B.; Cao, Y.; Xu, B.; Hou, L.; Guo, H.; Cheng, S.; Huang, G.; Zhang, C.; Sun, Q. Insight into the microstructural evolution of anthracite during carbonization-graphitization process from the perspective of materialization. *Int. J. Min. Sci. Technol.* **2022**, *32*, 1397–1406. [CrossRef]

24. Pusz, S.; Kwiecinska, B.K.; Duber, S. Textural transformation of thermally treated anthracites. *Int. J. Coal Geol.* **2003**, *54*, 115–123. [CrossRef]
25. Pusz, S.; Duber, S.; Kwiecinska, B.K. The study of textural and structural transformations of carbonized anthracites. *Fuel Process. Technol.* **2002**, *77*, 173–180. [CrossRef]
26. Li, J.; Qin, Y.; Chen, Y.; Shen, J. Microstructural Characteristics of Graphite Microcrystals in Graphitized Coal: Insights from Petrology, Mineralogy and Spectroscopy. *Minerals* **2022**, *12*, 1189. [CrossRef]
27. Rodrigues, S.; Marques, M.; Ward, C.R.; Suarez-Ruiz, I.; Flores, D. Mineral transformations during high temperature treatment of anthracite. *Int. J. Coal Geol.* **2012**, *94*, 191–200. [CrossRef]
28. Rodrigues, S.; Suarez-Ruiz, I.; Marques, M.; Flores, D. Catalytic role of mineral matter in structural transformation of anthracites during high temperature treatment. *Int. J. Coal Geol.* **2012**, *93*, 49–55. [CrossRef]
29. Finkelman, R.B.; Dai, S.; French, D. The importance of minerals in coal as the hosts of chemical elements: A review. *Int. J. Coal Geol.* **2019**, *212*, 103251. [CrossRef]
30. Yang, F.; Chen, H.; Guo, J.; Zheng, P. Catalytic graphitization of anthracite-derived carbon as the anode for Li/K-ion batteries. *J. Mater. Sci. -Mater. Electron.* **2022**, *33*, 4862–4868. [CrossRef]
31. Tang, L.; Mao, Q.; You, Z.; Yao, Z.; Zhu, X.; Zhong, Q.; Xiao, J. Catalytic graphitization in anthracite by reduced iron particles and investigating the mechanism of catalytic transformation via molecular dynamics. *Carbon* **2022**, *188*, 336–348. [CrossRef]
32. Mochida, I.; Ohtsubo, R.; Takeshita, K.; Marsh, H. Catalytic graphitization of graphitizable carbon by chromium, manganese and molybdenum oxides. *Carbon* **1980**, *18*, 25–30. [CrossRef]
33. Feng, B.; Bhatia, S.K.; Barry, J.C. Structural ordering of coal char during heat treatment and its impact on reactivity. *Carbon* **2002**, *40*, 481–496. [CrossRef]
34. Vlahov, A. XRD graphitization degrees: A review of the published data and new calculations, correlations, and applications. *Geol. Balk* **2021**, *50*, 11–35. [CrossRef]
35. Wu, Y.; Li, K.; Wang, Z.; Hu, M.; Cao, H.; Liu, Q. Fluctuations in Graphitization of Coal Seam-Derived Natural Graphite upon Approaching the Qitianling Granite Intrusion, Hunan, China. *Minerals* **2021**, *11*, 1147. [CrossRef]
36. Pappano, P.J.; Schobert, H.H. Effect of Natural Mineral Inclusions on the Graphitizability of a Pennsylvania Anthracite. *Energy Fuels* **2009**, *23*, 422–428. [CrossRef]
37. Ōya, A.; Fukatsu, T.; Ōtani, S.; Marsh, H. Catalytic graphitization of cokes by indigeneous mineral matter. *Fuel* **1983**, *62*, 502–507. [CrossRef]
38. Bonijoly, M.; Oberlin, M.; Oberlin, A. A possible mechanism for natural graphite formation. *Int. J. Coal Geol.* **1982**, *1*, 283–312. [CrossRef]
39. Evans, E.L.; Jenkins, J.L.; Thomas, J. Direct electron microscopic studies of graphitic regions in heat-treated coals and coal extracts. *Carbon* **1972**, *10*, 637–642. [CrossRef]
40. Badenhorst, C.; Santos, C.; Lazaro-Martinez, J.; Bialecka, B.; Cruceru, M.; Guedes, A.; Guimaraes, R.; Moreira, K.; Predeanu, G.; Suarez-Ruiz, I.; et al. Assessment of Graphitized Coal Ash Char Concentrates as a Potential Synthetic Graphite Source. *Minerals* **2020**, *10*, 986. [CrossRef]
41. Li, K.; Rimmer, S.M.; Liu, Q. Geochemical and petrographic analysis of graphitized coals from Central Hunan, China. *Int. J. Coal Geol.* **2018**, *195*, 267–279. [CrossRef]
42. Li, K.; Liu, Q.; Cheng, H.; Hu, M.; Zhang, S. Classification and carbon structural transformation from anthracite to natural coaly graphite by XRD, Raman spectroscopy, and HRTEM. *Spectrochim. Acta Part A-Mol. Biomol. Spectrosc.* **2021**, *249*, 119286. [CrossRef] [PubMed]
43. Quan, Y.; Liu, Q.; Li, K.; Zhang, H.; Yang, Y.; Zhang, J. Simultaneous fluorination and purification of natural block coaly graphite into fluorinated graphene with tunable fluorination degree. *Mater. Today Commun.* **2022**, *32*, 104130. [CrossRef]
44. Qiu, T.; Yang, J.-G.; Bai, X.-J. Investigation on microstructural changes of Anthracite during Graphitization and effect of Silica content on product crystal structure. *Energy Sources Part A-Recovery Util. Environ. Eff.* **2021**, *43*, 769–782. [CrossRef]
45. Wang, L.; Qiu, T.; Guo, Z.; Shen, X.; Yang, J.; Wang, Y. Changes and Migration of Coal-Derived Minerals on the Graphitization Process of Anthracite. *ACS Omega* **2021**, *6*, 180–187. [CrossRef]
46. Yuan, L.; Liu, Q.; Mathews, J.P.; Zhang, H.; Wu, Y. Quantifying the Structural Transitions of Chinese Coal to Coal-Derived Natural Graphite by XRD, Raman Spectroscopy, and HRTEM Image Analyses. *Energy Fuels* **2021**, *35*, 2335–2346. [CrossRef]
47. Quan, Y.; Liu, Q.; Zhang, S.; Zhang, S. Comparison of the morphology, chemical composition and microstructure of cryptocrystalline graphite and carbon black. *Appl. Surf. Sci.* **2018**, *445*, 335–341. [CrossRef]
48. Biscoe, J.; Warren, B. An x-ray study of carbon black. *J. Appl. Phys.* **1942**, *13*, 364–371. [CrossRef]
49. Laggoun-Défarge, F.; Lallier-Verges, E.; Suárez-Ruiz, I.; Cohaut, N.; Bautista, A.J.; Landais, P.; Prado, J. *Evolution of Vitrinite Ultrafine Structures during Artificial Thermal Maturation*; ACS Publications: Washington, DC, USA, 1994. [CrossRef]
50. Lu, L.; Sahajwalla, V.; Kong, C.; Harris, D. Quantitative X-ray diffraction analysis and its application to various coals. *Carbon* **2001**, *39*, 1821–1833. [CrossRef]
51. Seehra, M.S.; Pavlovic, A.S. X-Ray diffraction, thermal expansion, electrical conductivity, and optical microscopy studies of coal-based graphites. *Carbon* **1993**, *31*, 557–564. [CrossRef]
52. Zhang, H.; Li, K.; Sun, J.; Sun, Z.; Yuan, L.; Liu, Q. The structural evolution and mutation of graphite derived from coal under the influence of natural igneous plutonic intrusion. *Fuel* **2022**, *322*, 124066. [CrossRef]

53. Li, K.; Liu, Q.; Hou, D.; Wang, Z.; Zhang, S. Quantitative investigation on the structural characteristics and evolution of high-rank coals from Xinhua, Hunan Province, China. *Fuel* **2021**, *289*, 119945. [CrossRef]
54. Li, K.; Liu, Q.; Rimmer, S.M.; Huggett, W.W.; Zhang, S. Investigation of the carbon structure of naturally graphitized coals from Central Hunan, China, by density-gradient centrifugation, X-ray diffraction, and high-resolution transmission electron microscopy. *Int. J. Coal Geol.* **2020**, *232*, 103628. [CrossRef]
55. Shao, Y.; Wang, S.; Li, X. The Effect of Silicon-Containing Minerals on Coal Evolution at High-Temperature Pre-Graphitization Stage. *Minerals* **2023**, *13*, 20. [CrossRef]
56. Chen, G.; Cao, D.; Wang, A.; Wei, Y.; Liu, Z.; Zhao, M. A High-Temperature Thermal Simulation Experiment for Coal Graphitization with the Addition of SiO_2. *Minerals* **2022**, *12*, 1239. [CrossRef]
57. Burgess-Clifford, C.E.; Narayanan, D.L.; Van Essendelft, D.T.; Jain, P.; Sakti, A.; Lueking, A.D. The effect of calcination on reactive milling of anthracite as potential precursor for graphite production. *Fuel Process. Technol.* **2009**, *90*, 1515–1523. [CrossRef]
58. Neupane, B.; Ju, Y.; Silwal, B.R.; Singh, P.K.; Huang, C. Structural investigations of Eocene coals from foreland basin of central Nepal Himalaya. *Energy Explor. Exploit.* **2017**, *35*, 713–733. [CrossRef]
59. Zhang, Y.; Kang, X.; Tan, J.; Frostt, R.L. Influence of Calcination and Acidification on Structural Characterization of Anyang Anthracites. *Energy Fuels* **2013**, *27*, 7191–7197. [CrossRef]
60. Wang, L.; Cao, D.; Peng, Y.; Ding, Z.; Li, Y. Strain-Induced Graphitization Mechanism of Coal-Based Graphite from Lutang, Hunan Province, China. *Minerals* **2019**, *9*, 617. [CrossRef]
61. Zhang, S.; Liu, Q.; Zhang, H.; Ma, R.; Li, K.; Wu, Y.; Teppen, B.J. Structural order evaluation and structural evolution of coal derived natural graphite during graphitization. *Carbon* **2020**, *157*, 714–723. [CrossRef]
62. Zhang, S.; Song, B.; Cao, C.; Zhang, H.; Liu, Q.; Li, K.; Teppen, B.J. Structural Evolution of High-Rank Coals during Coalification and Graphitization: X-ray Diffraction, Raman Spectroscopy, High-Resolution Transmission Electron Microscopy, and Reactive Force Field Molecular Dynamics Simulation Study. *Energy Fuels* **2021**, *35*, 2087–2097. [CrossRef]
63. Chen, H.; Wang, S.; Zhang, X.; Zhao, Y.; Zhang, H. A study of chemical structural evolution of thermally altered coal and its effect on graphitization. *Fuel* **2021**, *283*, 119295. [CrossRef]
64. Huang, Q.; Wei, K.; Xia, H. A novel perspective of dolomite decomposition: Elementary reactions analysis by thermogravimetric mass spectrometry. *Thermochim. Acta* **2019**, *676*, 47–51. [CrossRef]
65. Zhu, T.Y.; Zhang, S.Y.; Hung, J.J.; Wang, Y. Effect of calcium oxide on pyrolysis of coal in a fluidized bed. *Fuel Process. Technol.* **2000**, *64*, 271–284.
66. Guan, R.G.; Li, W.; Li, B.Q. Effects of Ca-based additives on desulfurization during coal pyrolysis. *Fuel* **2003**, *82*, 1961–1966. [CrossRef]
67. Chen, H.K.; Li, B.Q.; Zhang, B.J. Decomposition of pyrite and the interaction of pyrite with coal organic matrix in pyrolysis and hydropyrolysis. *Fuel* **2000**, *79*, 1627–1631. [CrossRef]
68. Srinivasan, G.; Seehra, M.S. Effect of pyrite and pyrrhotite on free radical formation in coal. *Fuel* **1983**, *62*, 792–794. [CrossRef]